Journal of Electron Spectroscopy and Related Phenomena 230 (2019) 1–9

Contents lists available at ScienceDirect

Journal of Electron Spectroscopy and Related Phenomena

journal homepage: www.elsevier.com/locate/elspec

DFT calculations of energy dependent XPS valence band spectra

Mahdiyar Bagheri*, Peter Blaha

Institute of Materials Chemistry, Technical University Vienna, Vienna, A-1060 Austria

ARTICLE INFO

Keywords:
Density functional theory
APW
XPS
Valence bands
Orbital cross sections

ABSTRACT

In the past few years it became regularly possible to measure valence band X-ray photoelectron spectra (XPS) using variable excitation energies. This ranges from UV-light to conventional X-ray sources (like Al K_α) all the way to synchrotron radiation with energies of several keV. In order to explain the observed variations in intensity with respect to the excitation energy, we performed XPS calculations using the WIEN2k code. The new PES module computes the XPS spectra using a combination of partial density of states times excitation-energy-dependent atomic-orbital cross sections. It considers as additional correction the charge fraction of the corresponding orbital located inside the atomic spheres. The resulting XPS spectra are compared with experimental data for SiO_2, PbO_2, $CeVO_4$, In_2O_3 and ZnO at different excitation energies and in general good agreement between the simulated and experimental spectra has been achieved. In some cases significant unexpected contributions like Pb-6d in PbO_2 or Zn-4p in ZnO appear and explain some features in the experimental spectra which previously have not been identified.

1. Introduction

In the past decade first principle calculations of the electronic structure of solids based on density functional theory (DFT) was improved methodologically and several high quality computer codes were developed [1]. Among the many available packages, the WIEN2k [2] code, which is based on the augmented plane wave (APW) method, is among the most accurate schemes for band structure calculations. A key result of any DFT calculation is the total density of states (DOS) as well as its decomposition into partial DOS (PDOS) of different atoms and angular momentum character.

On the other hand, photoelectron spectroscopy is a very successful experimental technique to obtain information on the electronic structure of a material. Usually the so obtained valence photoelectron spectra are just interpreted by comparison with the theoretically calculated DOS, but this qualitative comparison has clear limitations. First of all, there is the fundamental problem that orbital energies in DFT are not excitation energies [3] and the corresponding DOS does not necessarily match experimentally measured spectra. Second, and even more important, such a simple comparison can never explain the sometimes significant dependency of the measured spectra on the energy of the incident UV or X-ray radiation. Recent developments of high intensity synchrotron generated X-ray sources unlocked the possibility of precise X-ray photoelectron spectroscopy (XPS) measurements at different excitation energies [4]. Synchrotron-based photoelectron spectroscopy using hard X-rays (HAXPES) has the advantage of being more bulk sensitive then conventional XPS and the linear dichroism in the angular distribution (LDAD) offers additional information. Thus, genuine calculations of energy dependent valence photoelectron spectra need to consider the interaction of the X-rays with the material at the specific excitation energy, the specific polarization and the particular geometrical setup. Together with appropriate atomic sub-shell photoionization cross sections this leads to an appropriate revision of the calculated DOS and can explain specific features appearing in XPS measurements with a particular setup.

A detailed description of the problem, the theoretical background and appropriate solutions to photo electron spectroscopy can be found in Ref. [5,6] with references to many other earlier work. It has been used in a couple of applications [7–13], but as far as we know no general and automatic program exists. In addition, to our knowledge a correction of the PDOS according to the corresponding localization has never been applied and we will demonstrate that this can be important in certain cases. In this article we give a summary to introduce the problem and use the theory to develop and test a new module for WIEN2k.

2. Theory

Earlier theoretical and experimental research has shown that one needs to sum up the contributions of individual orbital cross sections to

* Corresponding author.
E-mail address: bagheri.mahdiyar@tuwien.edu (M. Bagheri).

https://doi.org/10.1016/j.elspec.2018.11.002
Received 10 September 2018; Received in revised form 28 October 2018; Accepted 6 November 2018
Available online 10 November 2018
0368-2048/

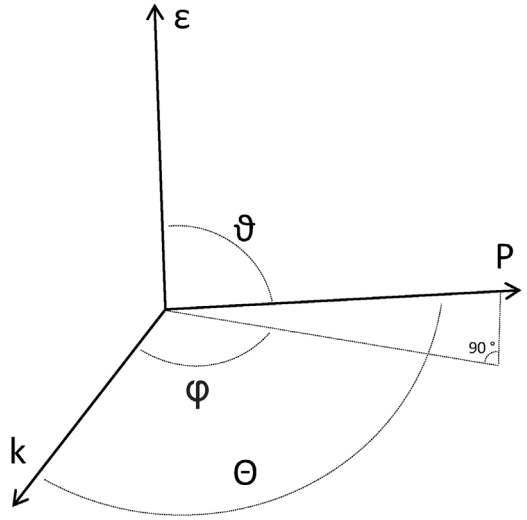

Fig. 1. Schematic representation of angles and directions of the photo ionization process. ***P*** and ***k*** are the photoelectron and photon propagation directions, ϵ is the direction of the photon polarization.

the total photo electron spectrum to explain a measured spectrum with reasonable high precisions [6]. Orbital cross sections describe the probability of the absorption of a photon of given energy leading to an excitation of an electron in a particular atomic sub-shell (orbital) and consequently the emission of this excited photoelectron. The differential cross section of photoelectrons of sub-shells i (see Ref. [5]) is given by

$$\frac{d\sigma_i(E,\vartheta,\varphi)}{d\Omega} = \frac{4\pi^2\alpha}{\omega}|D_{\mathrm{if}}|^2, \tag{1}$$

where E is the electron energy, ω is the photon frequency, α is the fine structure constant and ϑ, φ are angles between the photoelectron and the polarization and propagation of the photon, respectively (Fig. 1). Expanding the exponential term in the matrix element D_{if} between the initial (ψ_i) and final state (ψ_f) wave functions (in the non relativistic case) results in the well-known dipole and quadruple approximation [5]:

$$D_{\mathrm{if}} = <\psi_i^*|e^{i\boldsymbol{k}.\boldsymbol{r}}p_z|\psi_f> \tag{2}$$

$$D_{\mathrm{if}} = \omega < z > + \frac{i\omega^2\alpha}{2} < \mathrm{xz} > - \frac{\alpha\omega}{2} < L_y> \tag{3}$$

In these equations p denotes the momentum operator, $\omega < z >$ and $\omega^2 < xz >$ are the electric dipole and quadrupole matrix elements, while $< L_y >$ represents the magnetic dipole transition. Photon polarization ϵ and propagation ***k*** are assumed to be in z and x direction, respectively (Fig. 1). Within the electric dipole approximation, the differential cross section for unpolarized radiation can be written as [5]:

$$\frac{d\sigma_i}{d\Omega} = \frac{\sigma_i}{4\pi}\left[1 - \frac{\beta_i}{2}P_2(\cos\Theta)\right] \tag{4}$$

The i^{th} atomic sub-shell photoionization cross section σ_i is modified by an asymmetry angular distribution parameter β_i times a second order Legendre polynomial $P_2(cos\Theta)$, where Θ is measured between the propagation vector ***k*** of the incoming photon and the emitted photoelectron wave vector ***P***. At low excitation energies the asymmetry angular distribution parameter β_i plays the major role in correcting the cross section σ_i, however at high excitation energies this term is not sufficient and non-dipolar contributions are necessary [6]. Introducing two additional non-dipolar parameters γ_i and δ_i corresponding to quadrupole transitions, give a general expression for the differential photoionization cross section for unpolarized or circularly polarized (Eq. (5)) and linearly polarized (Eq. (6)) radiation:

$$\frac{d\sigma_i}{d\Omega} = \frac{\sigma_i}{4\pi}\left[1 - \frac{\beta_i}{2}P_2(\cos\Theta) + \left(\frac{\gamma_i}{2}\sin^2\Theta + \delta_i\right)\cos\Theta\right] \tag{5}$$

$$\frac{d\sigma_i}{d\Omega} = \frac{\sigma_i}{4\pi}[1 + \beta_i P_2(\cos\vartheta) + (\delta_i + \gamma_i\cos^2\vartheta)\sin\vartheta\cos\varphi] \tag{6}$$

Several authors have calculated the angular distribution parameters σ_i, β_i, γ_i and δ_i for all elements and atomic orbitals. We have used the tabulated parameters calculated by Trezhaskovskaya et al. [14,15]. These tables contain dipolar and non-dipolar atomic orbital sub-shell parameters of the elements for energies up to 10000 eV and we have used a linear interpolation to obtain the cross section for a particular energy. It has to be pointed out that the tabulated parameters have been calculated for completely filled shells of isolated atoms. In order to compute the total atomic cross section with the tabulated parameters, the experimental setup like X-ray polarization, X-ray and photoelectron propagation direction, detector acceptance angle etc. has to be considered.

For the general case of unpolarized (or circularly polarized) radiation integrating Eq. (5) around angle Θ between incoming photon and outgoing photoelectron results in a general form of the total atomic cross section:

$$I_i^{\mathrm{tot}} = \left[\frac{\sigma_i}{4\pi}[\Theta - \frac{\beta_i}{4}(\frac{1}{2}\Theta + \frac{3}{4}\sin 2\Theta) + \frac{\gamma_i}{2}(\frac{1}{3}\sin^3\Theta) + \delta_i\sin\Theta]\right]_{\Theta-\Delta}^{\Theta+\Delta} \tag{7}$$

The value of the angle Θ and the angular acceptance of the photo electron analyzer $\pm\,\Delta$ has to be chosen according to an explicit experiment. Most laboratory XPS incorporate unpolarized low energy X-ray sources and hence fall into above mentioned formalism. At this limit besides σ_i the asymmetry parameter β_i is the key factor of determining the total atomic cross section, while non-dipolar parameters γ_i and δ_i are typically between one to eight orders of magnitude smaller than σ_i and β_i and therefore play an insignificant role. Considering the most common low energy XPS experimental setups with photo electron take off angle of 90° and analyzer acceptance angle $\Delta = \pm\,15°$, we obtain:

$$I_i^{\mathrm{tot}} = \frac{\sigma_i}{4\pi}[1 - \frac{\beta_i}{8}] \tag{8}$$

Eq. (8) has been employed in the new module as default formula for unpolarized (or circularly polarized) radiation. It is easy to verify that Eq.(8) is rather insensitiv to small changes of the photoelectron take off or acceptor angles and thus this equation could be considered as a very good approximation for a wide range of common low energy unpolarized (or circularly polarized) XPS experiments.

Moving on to linearly polarized X-rays Mudd et al. [9] has given a simple expression for the total cross section (Eq. (9)) assuming that the angle φ, which is between photon propagation direction ***k*** and the plane defined by electron emission ***P*** and polarization vector ϵ, is fixed to zero in the experiment. Such geometries and other similar situations [11] have no quadrupolar dependency and the parameters γ and δ vanish due to integration over symmetric ϑ ranges and the odd parity of the non-dipolar terms. For instance using an angular acceptance angle of the electron analyzer of ± 30° the total cross section of sub-shell i can be written as:

$$I_i^{\mathrm{tot}} = \frac{\sigma_i}{96\pi}[8\pi + \beta_i(9\sqrt{3} + 2\pi)] \tag{9}$$

Photoelectron spectra generated by linearly polarized X-ray sources can be measured parallel or perpendicular to the polarization of the electric field vector of the X-ray source. Quardi et al. [7] used this specific experimental setup (parallel and perpendicular detection of photoelectron) along with linear dichroism in angular distribution (LDAD) of photoelectrons to derive another set of expressions for the total atomic cross section. Within the dipole approximation the LDAD intensity (Eq. (12)) has been defined as the intensity difference between parallel (Eq. (10)) and perpendicular (Eq. (11)) detection geometries.

$$I_i^{\text{parallel}} \propto \sigma_i(1 + \beta_i) \tag{10}$$

$$I_i^{\text{perpendicular}} \propto \sigma_i\left(1 - \frac{\beta_i}{2}\right) \tag{11}$$

$$I_i^{\text{LDAD}} \propto \sigma_i\left(\frac{3\beta_i}{2}\right) \tag{12}$$

Including non-dipolar terms, the parallel photoelectron intensity remains the same but the perpendicularly measured photoelectron spectra is modified by δ_i corresponding to a quadrupole transition.

$$I_{\text{nl}}^{\text{perpendicular}} \propto \sigma_i\left(1 - \frac{\beta_i + \delta_i}{2}\right) \tag{13}$$

In order to include specific experimental geometry setups used for parallel and perpendicular measurements, we have followed Nefedov et al. [16] to calculate the polarization dependent total atomic cross sections. In the limit of Θ equal to 90° one obtains Eqs.(10) and (11) for the total atomic cross sections of linearly polarized radiation by neglecting the non-dipolar terms and fixing the angles ϑ, φ to 0° for parallel and ϑ, φ to 90° for perpendicular measurements of the emitted photoelectrons. In order to simulate the HAXPES experiments for ZnO, we have used Eq.(6) and applied the experimental geometry setup specified for parallel and perpendicular polarized measurements (acceptance angles of the photo detector as ± 15.3° for parallel and ± 3.5° for perpendicular polarization, see [17], [11]). Then the total atomic cross sections are given by:

$$I_i^{\text{parallel}} \propto \sigma_i/4\pi(1 + 0.35\beta_i + 0.65\delta_i + 0.37\gamma_i) \tag{14}$$

$$I_i^{\text{perpendicular}} \propto \sigma_i/4\pi(1 - 0.47\beta_i - 0.019\delta_i - 0.0003\gamma_i) \tag{15}$$

Obviously other specific expressions for the total atomic cross sections can be derived for different experimental setups, but we have implemented Eqs. (8)–(15) into our new PES module.

In a solid the initial valence states i are represented by the corresponding PDOS and in order to calculate the energy and setup dependent XPS spectrum these PDOS are multiplied with the corresponding cross-sections as derived above and summed over all atoms and orbitals. In the APW method as implemented in the WIEN2k code [2] the unit cell is decomposed into non-overlapping atomic spheres (centered at the atomic sites) and an interstitial region. In the interstitial region we use plane waves as basis set and a decomposition of the interstitial part of the wave function into atomic orbital contributions is not uniquely possible. Thus the atomic PDOS is calculated only using contributions from inside the sphere and the total DOS is *not* the sum of all atomic PDOS, but the interstitial PDOS must also be added. This interstital PDOS, however, cannot be assigned to specific atomic orbitals without further approximations. Naturally, the PDOS of localized orbitals (like 3d states of transition metals) will be almost complete, but more delocalized states (in particular the valence s and p states of transition metals) have only a small fraction (sometimes only 10 % or even less) of their charge inside the corresponding atomic sphere and most of their charge will be in the interstital. The corresponding PDOS is therefore much too small and we correct for this in an approximate way by multiplication of the PDOS with the inverse charge fraction of the corresponding orbital in a free atom. In the free atom the occupation of an orbital is known (e.g. 1 electron for Na-3s) and the corresponding charge inside the atomic sphere (with the same radius as in the bulk) can be calculated easily. In addition we rescale these "inverse charge fraction" weights slightly, such that the least square fit of the sum of the weighted PDOS is as close as possible to the total DOS. This accounts for small contractions/expansions of atomic orbitals in the solid.

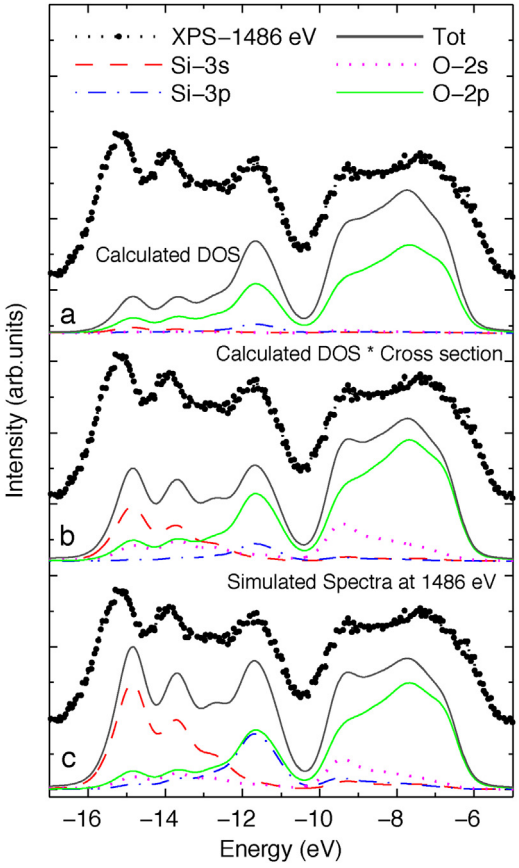

Fig. 2. SiO_2 valence band XPS at 1486 eV [8] in comparison to: a) the partial and total calculated DOS, b) the partial and total simulated spectra taking into account the atomic cross sections, c) and the final simulated XPS spectra including the additional weighting of the PDOS with their inverse charge fraction inside the atomic spheres.

3. Computations

All the calculations have been carried out using the APW + local orbitals method as implemented in WIEN2k [2]. In case of SiO_2, In_2O_3 and PbO_2 the calculations were performed with the Perdew-Burke-Ernzerhof (PBE) generalized gradient approximation (GGA) [18]. In case of $CeVO_4$ and ZnO the calculation were performed by PBE + U [19]. All calculations are well converged with respect to basis set and k-point samplings. In order to simulate XPS spectra the calculated DOS has been broadened with a Lorentzian (0.1 eV to account for life-time broadening) and a Gaussian of full-width-half-maximum equals to 1.05, 0.70, 0.36, 0.80 and 0.70 eV for SiO_2, PbO_2, In_2O_3, $CeVO_4$ and ZnO, respectively. For each example the total atomic cross section has been calculated considering the experimental set up presented in the corresponding experiment. In case of SiO_2, PbO_2 and $CeVO_4$ total atomic cross sections have been calculated by Eq.(8). For the In_2O_3 example Eq.(10) (for tests also Eq.(9)) and for ZnO Eq.(14)-(15) have been used.

4. SiO_2

Fig. 2.a shows valence band photoelectron spectra of alpha quartz SiO_2 measured at 1486 eV [8] in comparison to the DFT calculated DOS and its orbital constituents. A quick comparison between the calculated total DOS, which is dominated by O-2p contributions, and the XPS spectrum reveals that although the calculated DOS peak positions agree well with experiment, the XPS intensities are very badly reproduced, in particular at lower energies. In a first step we simulate the XPS spectrum by summing up all PDOS contributions multiplied with their

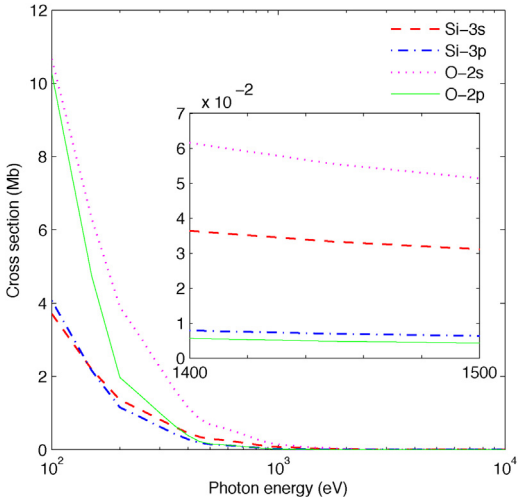

Fig. 3. Photoionization cross sections of Si-3s, Si-3p, O-2s and O-2p. The inset shows an enhanced view for a small energy region of 1400-1500 eV.

corresponding orbital cross sections (Fig. 2.b) at 1486 eV according to Eq. (9). Since the Si-3s and O-2s cross sections at this energy are significantly larger (Fig. 3) than the Si-3p and O-2p cross sections, the corresponding PDOS contributions to the spectrum get a bit enhanced between -11 to -17 eV.

Nevertheless, the agreement with experiment is still not very good, because the Si-3s PDOS is simply too small. Taking into account that only about 25 % of the Si-3s but 76 % of O-2p charge is located inside the atomic spheres (with radii of 1.6 and 1.43 bohr, respectively), we get a dramatic increase of the Si-3s contribution to the XPS spectrum when we weight the corresponding PDOS with the inverse of the fraction of charge located inside the atomic spheres. The final simulated XPS spectrum (Fig. 2c) matches the XPS intensity very well. The Si-3s contribution becomes the dominant contribution for the two lowest XPS peaks, O-2p still dominates at higher energies. Si-3p contributes strongly to the peak located around −11.5 eV and O-2s contributions are very important for the peak at −9.3 eV.

At around −25 eV the experimental XPS spectrum (Fig. 4a) has a dominating peak centered around -25 eV of much larger intensity than the valence band. The calculated DOS shows strong O-2s contribution (Fig. 4b) at this peak position, but as expected the relative intensity of the peaks are poorly reproduced. On the other hand the simulated XPS spectrum (Fig. 4c) taking into account the orbital cross sections and the corresponding charge fractions matches the experimental XPS intensities very well. Note that it is well known that the binding energies

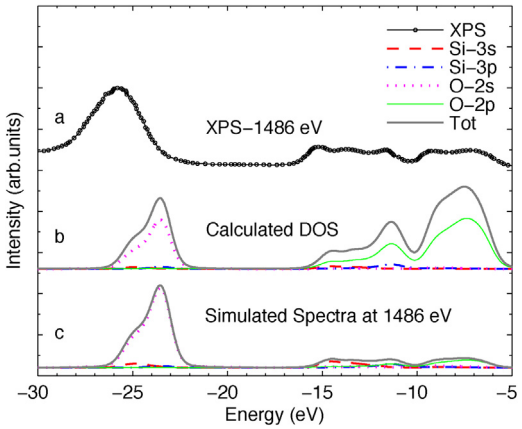

Fig. 4. a) SiO2 valence band XPS at 1486 eV [8] in comparison to: b) the partial and total calculated DOS, c) the simulated XPS spectrum.

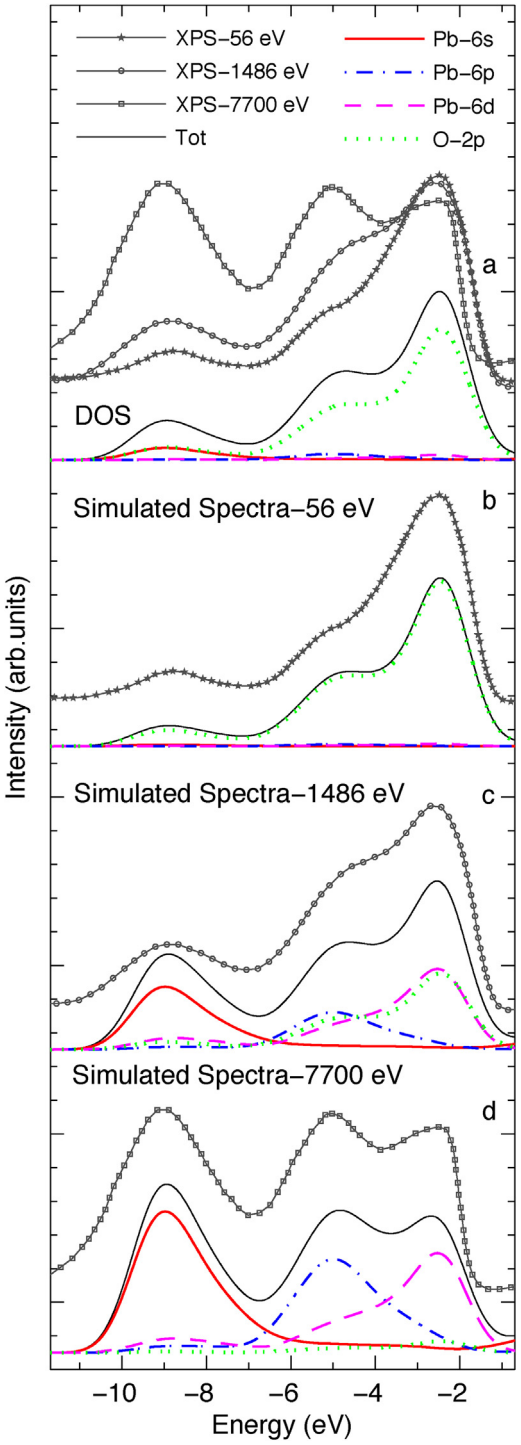

Fig. 5. PbO_2 valence band XPS at 56, 1486 and 7700 eV [10] in comparison to a) the total and partial DOS, b) the partial and total simulated XPS spectrum at 56 eV, c) at 1486 eV and d) at 7700 eV.

(BE) of the O-2s states is too low compared to experiment, because DFT eigenvalues must not be interpreted as excitation energies.

5. PbO_2

In this section we have examined the calculated valence band spectra of β-PbO_2, which crystallizes in the tetragonal rutile structure at 56, 1486 and 7700 eV excitation energy. The experimental XPS data have been taken from [10], where also some theoretical work about

energy dependent valence XPS has been presented similarly to our work. However, they neglected important Pb-6d contributions and thus could not explain properly the highest energy data. As can be seen in Fig. 5a the XPS spectra of PbO_2 consist of three major peaks, but their relative intensities strongly depend on the employed X-ray energy.

In any case, for all excitation energies the main peaks of the total DOS, which is dominated by O-2p states, agree well with the experimental peak positions, but fails to reproduce the XPS intensity profiles except at 56 eV. For this low excitation energy, the cross sections of Pb orbitals are very low and the spectrum can be explained by the O-2p contributions alone (Fig. 5b). At 1486 eV (Fig. 5c) the peak around −2 eV has still the largest intensity, but the peaks centered at −5 eV and −9 eV have gained weight. The intensities of our simulated spectrum nicely agrees with experiment and we can identify the individual contributions. The highest energy peak still has O-2p contributions but Pb-6d is even more important. For the middle peak Pb-6p, Pb-6d and O-2p contributions are important, while the lowest peak originates mainly from Pb-6s. All Pb contributions are strongly enhanced by their cross sections as compared to O-2p. Interestingly, there is also a strong Pb-6d contribution at the valence band maximum. Pb-5d states are real core states, but 6d orbitals are not occupied in a free Pb atom. In order to obtain cross section parameters for Pb-6d, we extrapolated the cross sections of neighboring elements containing 6d states in the free atom (Ac, Th, Pa) to the Pb atom.

Increasing the excitation energy further to 7700 eV (Fig. 5d) the relative intensities of the 3 peaks are reversed and the lowest energy peak dominates. The decomposition of the theoretical spectrum reveals that in particular the Pb-6s and the Pb-6p intensities are strongly enhanced and O-2p states play a negligible role for this spectrum. The peak around −2 eV is now dominated by Pb-6d contributions, which would be hardly visible in a PDOS alone and this is the reason why it was missed in previous simulations [10].

The energy dependency of XPS cross sections has been discussed by several authors before [5,6,14,10]. In general with higher excitation energy the cross sections of orbitals with a more uniform radial distribution (from lighter atoms, e.g. O-2p) decrease in contrast to orbitals, which have a rich oscillatory behavior in their radial distribution, as e,g. Pb-6s or 6p functions.

The experimental spectra do not end at the top of the O-2p valence band, but show an about 1.3 eV broad low intensity tail (Fig. 8 in reference [10]. This has been explained by n-type doping (O vacancies), which effectively shifts the Fermi edge into the conduction band. If we take this into account in our simulations and shift our Fermi energy up by 1.3 eV, we can very well reproduce this fine experimental detail. In the UPS spectra (Fig. 6a) and c)) this intensity originates solely form O-2p character, while at 7700 eV (Fig. 6b and d) it comes mainly from Pb-6s states.

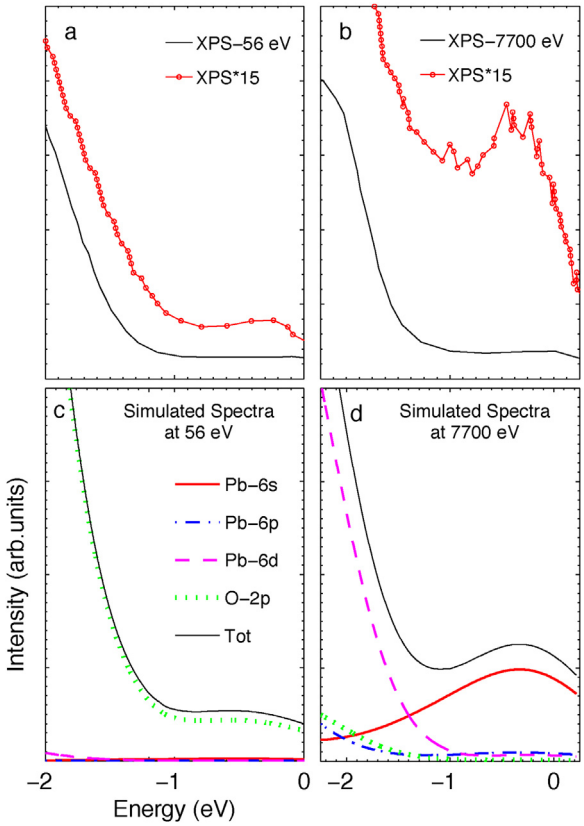

Fig. 6. Zoom in of the PbO_2 valence band XPS at 56 (a) and 7700 eV (b) [10] near the valence band maximum in comparison to the total simulated XPS spectrum at 56 (c) and 7700 eV (d). The theoretical Fermi energy has been shifted up by 1.3 eV to account for oxygen vacancies.

6. $CeVO_4$

In this example the simulated spectra of $CeVO_4$ in Zircon-type structure (space group $I4_1/amd$) has been examined against valence XPS at 1486 eV. The experimental XPS data has been taken from [13], where also simulated spectra have been presented. In order to calculate the spectra we have performed DFT calculation on anti-ferromagnetic $CeVO_4$ with the PBE+U functional for exchange and correlation treatment. A moderate U value of 2.7 eV has been applied to the 4f orbitals of Ce providing good agreement with experiment. It should be mentioned, that significant larger U values (for instance 4.5 eV for Ce-4f and 4 eV for V-3d as used in Ref.[13]) lead to a misalignment of the O-2p peak by 1 eV. As can be seen in Fig. 7a the XPS spectra of $CeVO_4$ consist of two major peaks, where the peak centered at −5.3 eV has shoulders on the low and high energy side. The total DOS (Fig. 7b), which is mainly dominated by O-2p and Ce-4f orbitals, agrees reasonable well with the XPS peak positions but fails to reproduce the relative intensities of the O-2p and Ce-4f peaks. In a first step we correct the intensities by multiplication of the PDOS with their corresponding atomic cross sections (Fig. 7c). In order to obtain the Ce-4f cross section we have carefully interpolated the cross section data of neighboring elements (La-4f, Sm-4f) and used it to calculate the Ce-4f cross section. Nevertheless, at the given excitation energy the large Ce-4f cross section overestimates the intensity of the Ce-4f peak centered at about −1.3 eV in agreement with the simulations presented in [13], where the disagreement was explained by " intensity borrowing" and a breakdown of the independent electron approximation. However, note that the Ce-4f charge is almost entirely located inside the corresponding atomic sphere, while this is not true for V-3d, O-2p and in particular V-4s states. Thus we have to weight the corresponding PDOS by the inverse of their charge contained inside the atomic spheres (Fig. 7d). This enhances the intensity of the lower energy peak in agreement with experiment. In addition a (small) maximum around -5 eV appear which originates from additional V-4p contributions, while the low and high BE shoulders stem from V-3d, O-2p and Ce-5d contributions. The simulated spectrum of $CeVO_4$ shows now very good agreement with experiment.

7. In_2O_3

In this section we investigate the electronic structure of In_2O_3 in the cubic bixbyite structure and compare it against experimental valence band spectra obtained from conventional Al K_α (1486 eV) laboratory sources and HAXPES (6000 eV). The experimental data have been taken from [20] and this article also presents a comparison with theoretically calculated energy dependent cross section weighted DOS at 1486 and 6000 eV, which we hope to improve in our final simulated spectra by taking into account the corresponding orbital charge fractions inside the atomic spheres. A quick comparison of the calculated DOS against

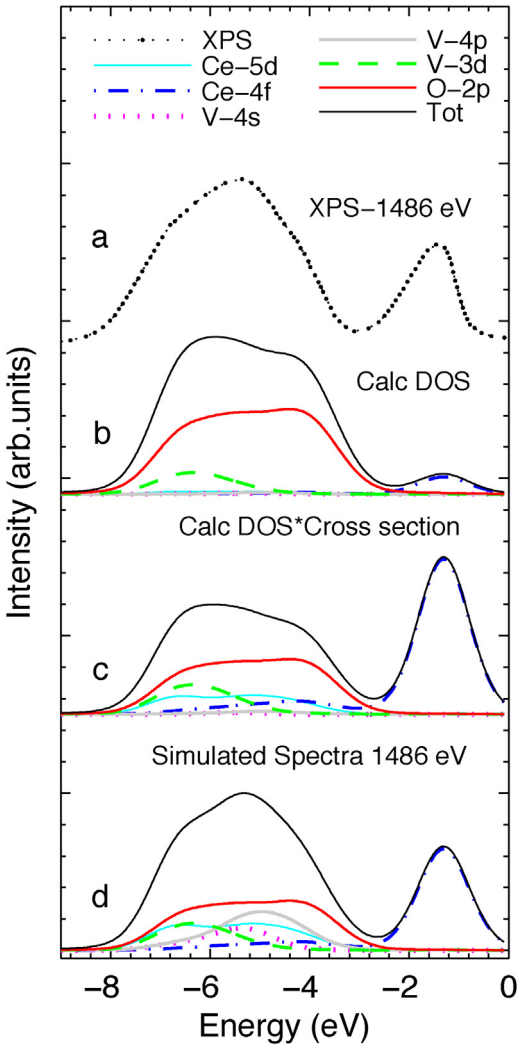

Fig. 7. a) $CeVO_4$ valence band XPS at 1486 eV in comparison to: b) DFT calculated DOS c) the partial and total simulated DOS taking into account the atomic cross section d) and the final simulated spectra.

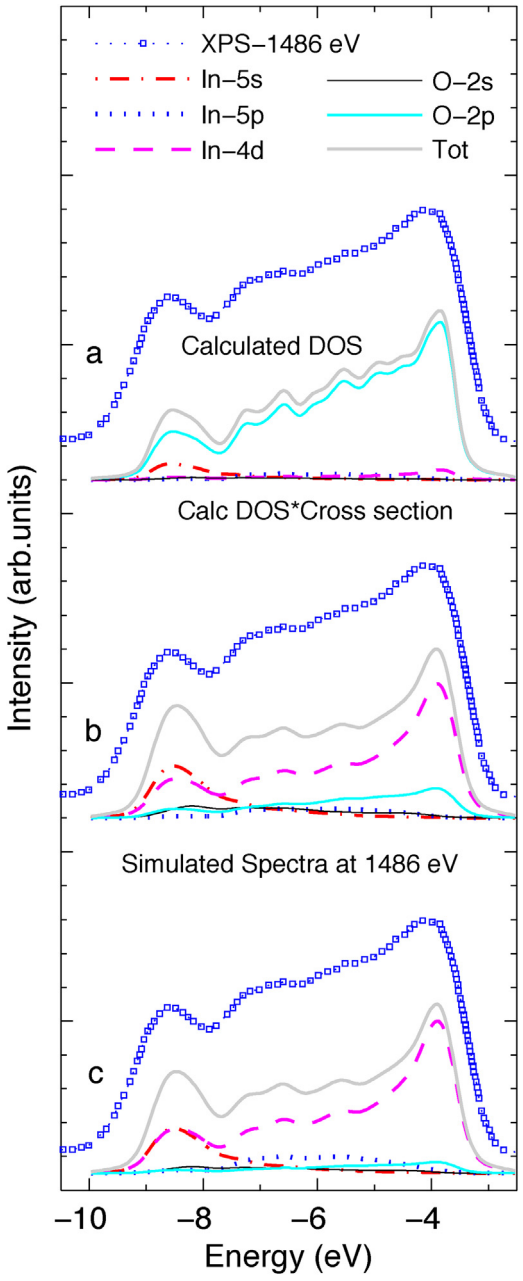

Fig. 8. In_2O_3 valence XPS at 1486 eV ([20]) in comparison to: a) the partial and total calculated DOS; b) the partial and total simulated spectra taking into account the atomic cross section; and c) the final simulated spectra including additional weighting of the PDOS with their inverse charge fraction inside the atomic spheres.

experimental XPS and HAXPES spectra (Fig. 8a and Fig. 9a) shows that the position of calculated DOS peaks is in good agreement with the observed valence spectra at both excitations. The intensities of the calculated DOS peaks shows also good agreement with XPS at 1486 eV but it clearly falls short to match HAXPES (6000 eV) peak intensities. Continuing with the first step of correction at 1486 eV, the cross section weighted DOS reveals a very similar spectrum, but the interpretation changes dramatically (Fig. 8a-b). While the total DOS is clearly dominated by O-2p character with small admixture of In-5s at low energies, in the cross section weighted spectra, contributions from In-4d dominate with some admixture of O-2p at higher energies (−3 to −7 eV) and In-5s at lower energies (−7 to −10 eV). Including now also the charge fraction correction the final simulated spectrum at 1486 eV (Fig. 8c) has a reduced O-2p and an increased In-5p contribution (since its charge is only 0.21 %). We have to mention that the final simulated spectrum still does not deliver the exact XPS intensities, and we trace this back to the usage of the atomic In-4d cross section. In fact, the In-4d states are more than 20 eV below the valence band and it is not fully justified to use the In-4d cross section for these more delocalized (5d-like) d states in the valence band.

In the case of the HAXPES spectrum, the calculated DOS with dominating O-2p character does not deliver a meaningful intensity profile at all. (Fig. 9a). Adding atomic cross sections to the PDOS (Fig. 9b) helps improve the intensity of the major peak located between −7 to −10 eV due to the rather large In-5s cross section at the given excitation energy. This result is very similar to the theoretical spectrum presented in Ref.[20]. However, when taking into account the orbital charge fractions inside the atomic spheres, the final simulated spectrum (Fig. 9 c) matches the HAXPES intensity profile very well, mainly due to the relative enhancement of In-5p contribution. As mentioned before Fig. 8a and Fig. 9a has been calculated using Eq.(10), but we have also examined this example with cross sections calculated by Eq.(9) (unpolarized radiation) and the simulated spectra for both excitation energies (1486 and 6000 eV) look very similar to the results presented here.

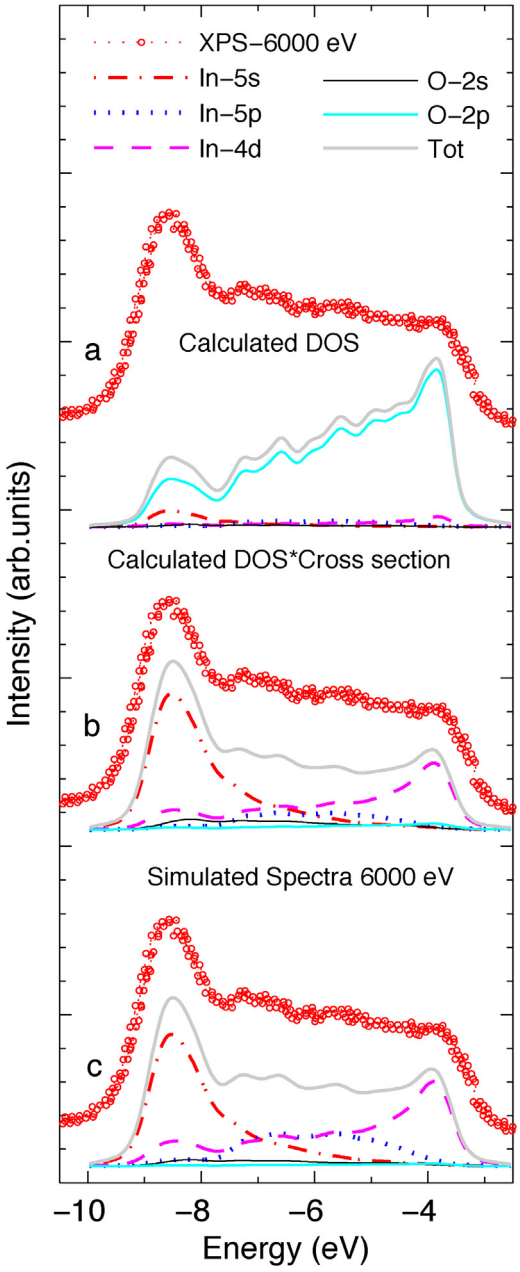

Fig. 9. In_2O_3 valence XPS at 6000 eV ([20]) in comparison to: a) the partial and total calculated DOS; b) the partial and total simulated spectra taking into account the atomic cross section; and c) the final simulated spectra including additional weighting of the PDOS with their inverse charge fraction inside the atomic spheres.

8. ZnO

In this example we calculate and compare the XPS spectra of wurtzite ZnO measured with conventional XPS (1486 eV) but also with linearly polarized HAXPES (7600 eV) measured at parallel and perpendicular experimental geometry setups using Eq. (14) and(15). More details about the XPS and HAXPES experiment, different geometrical setups and the measurement technique can be found in [17].

Let us start out with a rough comparison of peak positions between experimental spectra and the theoretical DOS (Fig. 10). It is obvious that the theoretical bandwidth is much too small when using the standard PBE approximation and the position of the 3d bands is at nearly 2 eV too low binding energy. It is well known in the DFT community that transition metal compounds (oxides) are not well described

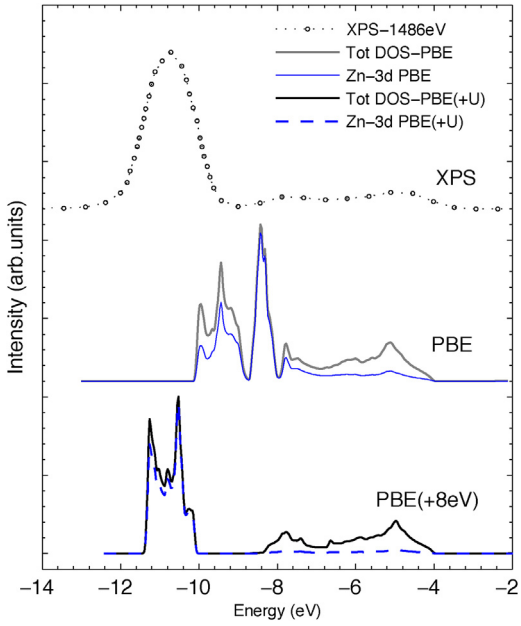

Fig. 10. Calculated total DOS and Zn-3d PDOS of ZnO using PBE and PBE + U approximations. A U value of 8 eV (for Zn-3d) has been applied to reach agreement with the experimental band width.

by a standard DFT approach, and one way to improve is to add a mean field Hubbard term for the correlated 3d electrons (DFT + U). When we perform PBE + U calculations with a U of 8 eV for the Zn-3d states, the 3d PDOS is shifted down by nearly 2 eV and aligns pretty well with the experimental spectrum (Fig. 10). All the following theoretical spectra will use these PBE + U calculations. The calculated DOS of ZnO (Fig. 11 a) has three major peaks. The first two peaks with maxima located around −5 eV and −7.5 eV have strong O-2p character, while the dominating last peak around −10.6 eV shows strong Zn-3d character. As expected the positions of these DOS peaks (in the PBE + U approximation) are in good agreement with experiment (XPS and HAXPES), but the calculated DOS cannot describe the intensity profile of any of the experimentally obtained valence band photoelectron spectra.

At 1486 eV (Fig. 11b) Zn-3d contributions dominate the valence band spectra, since the Zn-3d cross section is one and two orders of magnitude larger than the Zn-4s/4p and O-2p cross sections, respectively. Therefore the first two low BE peaks of the simulated spectra around -5 and -7.5 eV reduce their intensity considerably in comparison to the calculated DOS.

Moving on to the HAXPES spectra a special treatment of the photoelectron polarization dependency is necessary. The simulated HAXPES spectra for parallel and perpendicular setup are shown in Fig. 11c and Fig. 11d, respectively. The simulated parallel HAXPES spectra show virtually no contributions from O-2p anymore (because of the low cross section at this energy), but the three peaks located about −10.6 eV, -7.5 eV and -5 eV originate mainly from Zn-3d, Zn-4s and – surprisingly – Zn-4p, respectively. The Zn-4p contribution is rather unexpected as Zn does not have occupied 4p states in the free atom and the corresponding PDOS is still rather small. However, since the majority of the Zn-4p charge lies outside the atomic sphere a large enhancement arises and together with a significant cross section leads to the peak around -5 eV in good agreement with experiment. It should be mentioned that atomic cross sections for Zn-4p are not available, but we have carefully extrapolated them from the data of the neighboring elements Ga and Ge.

On the other hand the simulated HAXPES for perpendicular polarization (Fig. 11 d) shows a dramatic reduction of the Zn-4s intensity (and to a smaller extend also of the Zn-4p contributions), leading to much smaller peaks around -7.5 and -5 eV.

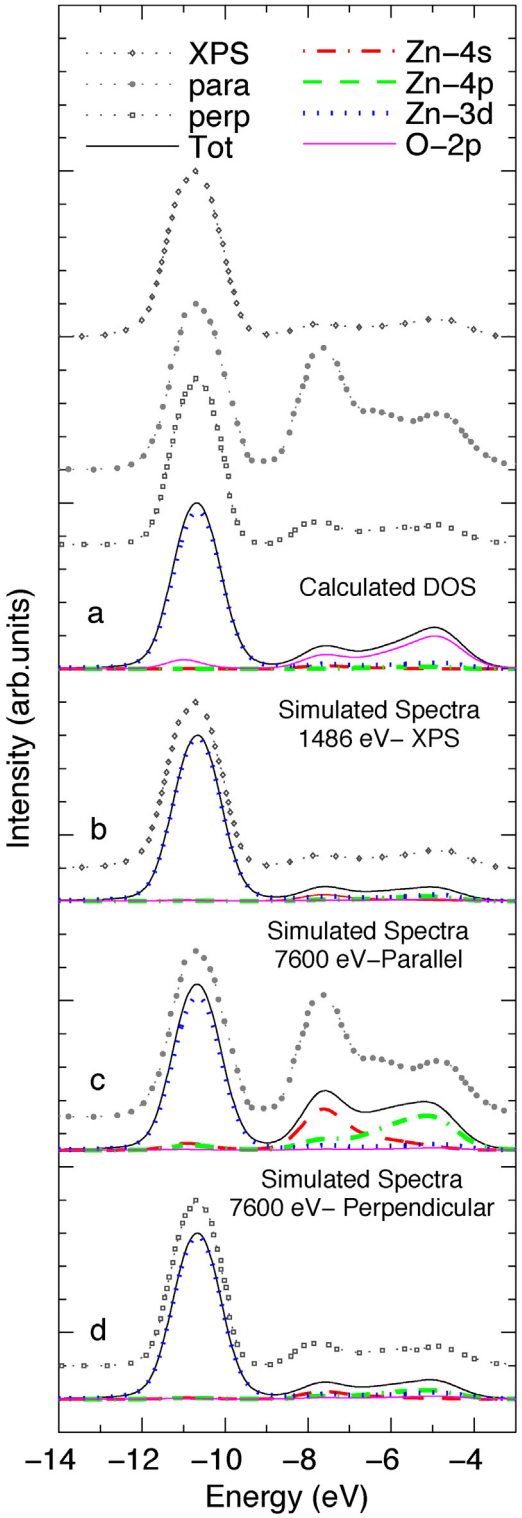

Fig. 11. Valence XPS (at 1486 eV) and HAXPES (7600 eV with parallel and perpendicular polarization setups) of ZnO compared with a) the partial and total calculated DOS b) the partial and total simulated spectra at 1486 eV c) at 7600 eV with parallel polarization d) at 7600 eV with perpendicular polarization. For all theoretical spectra the Zn-3d cross section has been reduced by an order of magnitude as compared to their tabulated values.

9. Conclusion

Accurate simulation of valence band photoemission spectra of solids requires to take into account the polarization and energy dependency of the observed photoelectrons. The valence band XPS spectra of SiO_2, PbO_2, $CeVO_4$, In_2O_3 and ZnO and the dependency on the excitation energy has been investigated using theoretical DFT calculations, which take the cross section modified PDOS as well as the localization of the different orbitals within their atomic spheres into account. The latter correction, which has never been considered before, changes the intensities in some cases significantly and comparison with experimental data validates the approach. Unexpected features like significant Pb-6d contributions in PbO_2 or Zn-4p contributions in ZnO have been detected leading to better agreement with experiment than previous simulations. Our approach can also reproduce the intensity ratio of Ce-4f to delocalized electron related peaks correctly in $CeVO_4$ simulated spectra.

Acknowledgment

We would like to thank Tomoyuki Yamamoto for his initial suggestions to take atomic orbital dependent cross-sections into account. This work was supported by the Austrian Science Fund (FWF) in project SFB-F41 (ViCoM) and the Vienna Scientific Cluster.

References

[1] Kurt Lejaeghere, Gustav Bihlmayer, Torbjörn Björkman, Peter Blaha, Stefan Blügel, Volker Blum, Damien Caliste, Ivano E. Castelli, Stewart J. Clark, Andrea Dal Corso, Stefano de Gironcoli, Thierry Deutsch, John Kay Dewhurst, Igor Di Marco, Claudia Draxl, Marcin Dułak, Olle Eriksson, José A. Flores-Livas, Kevin F. Garrity, Luigi Genovese, Paolo Giannozzi, Matteo Giantomassi, Stefan Goedecker, Xavier Gonze, Oscar Grånäs, E.K.U. Gross, Andris Gulans, François Gygi, D.R. Hamann, Phil J. Hasnip, N.A.W. Holzwarth, Diana Iuşan, Dominik B. Jochym, François Jollet, Daniel Jones, Georg Kresse, Klaus Koepernik, Emine Küçükbenli, Yaroslav O. Kvashnin, Inka L.M. Locht, Sven Lubeck, Martijn Marsman, Nicola Marzari, Ulrike Nitzsche, Lars Nordström, Taisuke Ozaki, Lorenzo Paulatto, Chris J. Pickard, Ward Poelmans, Matt I.J. Probert, Keith Refson, Manuel Richter, Gian-Marco Rignanese, Santanu Saha, Matthias Scheffler, Martin Schlipf, Karlheinz Schwarz, Sangeeta Sharma, Francesca Tavazza, Patrik Thunström, Alexandre Tkatchenko, Marc Torrent, David Vanderbilt, Michiel J. van Setten, Veronique Van Speybroeck, John M. Wills, Jonathan R. Yates, Guo-Xu Zhang, Stefaan Cottenier, Reproducibility in density functional theory calculations of solids, Science 351 (6280) (2016).

[2] P. Blaha, K. Schwarz, G.K.H. Madsen, D. Kvasnicka, J. Luitz, R. Laskowski, F. Tran, L.D. Marks, WIEN2k: An Augmented Plane Wave plus Local Orbitals Program for Calculating Crystal Properties, Vienna University of Technology, Austria, 2018.

[3] J.F. Janak, Proof that $\delta e/\delta n = \epsilon$ in density-functional theory, Phys. Rev. B 18 (1978) 7165–7168.

[4] Charles S. Fadley, Angle-resolved X-ray photoelectron spectroscopy, Prog. Surf. Sci. 16 (1984) 275–388.

[5] J.W. Cooper, Multipole corrections to the angular distribution of photoelectrons at low energies, Phys. Rev. A 42 (1990) 6942–6945.

[6] J.W. Cooper, Photoelectron-angular-distribution parameters for rare-gas subshells, Phys. Rev. A 47 (1993) 1841–1851.

[7] Siham Ouardi, Gerhard H. Fecher, Claudia Felser, Bulk electronic structure studied by hard X-ray photoelectron spectroscopy of the valence band: The case of intermetallic compounds, J. Electron Spectrosc. Relat. Phenom. 190 (2013) 249–267.

[8] V.P. Zakaznova-Herzog, H.W. Nesbitt, G.M. Bancroft, J.S. Tse, X. Gao, W. Skinner, High-resolution valence-band XPS spectra of the nonconductors quartz and olivine, Phys. Rev. B 72 (2005) 205113.

[9] J.J. Mudd, V. Tien-Lin Lee, Muñoz Sanjosé, J. Zúñiga Pérez, D.J. Payne, R.G. Egdell, C.F. McConville, Valence-band orbital character of CdO: A synchrotron-radiation photoelectron spectroscopy and density functional theory study, Phys. Rev. B 89 (2014) 165305.

[10] D.J. Payne, G. Paolicelli, F. Offi, G. Panaccione, P. Lacovig, G. Beamson, A. Fondacaro, G. Monaco, G. Vanko, R.G. Egdell, A study of core and valence levels in β-PbO_2 by hard X-ray photoemission, J. Electron Spectrosc. Relat. Phenom. 169 (1) (2009) 26–34.

[11] J. Weinen, T.C. Koethe, C.F. Chang, S. Agrestini, D. Kasinathan, Y.F. Liao, H. Fujiwara, C. Schüßler-Langeheine, F. Strigari, T. Haupricht, G. Panaccione, F. Offi, G. Monaco, S. Huotari, K.-D. Tsuei, L.H. Tjeng, Polarization dependent hard X-ray photoemission experiments for solids: Efficiency and limits for unraveling the orbital character of the valence band, J. Electron Spectrosc. Relat. Phenom. 198 (2015) 6–11.

[12] G. Panaccione, G. Cautero, M. Cautero, A. Fondacaro, M. Grioni, P. Lacovig, G. Monaco, F. Offi, G. Paolicelli, M. Sacchi, N. Stojic, G. Stefani, R. Tommasini, P. Torelli, High-energy photoemission in silver: resolving d and sp contributions in valence band spectra, J. Phys.: Condens. Matter 17 (17) (2005) 2671.

[13] J.P. Allen, Natasha Galea, Graeme Watson, Robert Palgrave, J.M. Kahk, David Payne, M.D.M. Robinson, G. Field, Anna Regoutz, Russell Egdell, Valence states in $CeVO_4$ and $Ce_{0.5}Bi_{0.5}VO_4$ probed by density functional theory calculations and X-ray photoemission spectroscopy, J. Phys. Chem. C 118 (44) (2014) 25330–25339.

[14] M.B. Trzhaskovskaya, V.I. Nefedov, V.G. Yarzhemsky, Photoelectron angular distribution parameters for elements Z = 1 to Z = 54 in the photoelectron energy range 100–5000 eV, At. Data Nucl. Data Tables 77 (1) (2001) 97–159.
[15] M.B. Trzhaskovskaya, V.K. Nikulin, V.I. Nefedov, V.G. Yarzhemsky, Non-dipole second order parameters of the photoelectron angular distribution for elements Z = 1 - 100 in the photoelectron energy range 1 - 10 keV, At. Data Nucl. Data Tables 92 (2) (2006) 245–304.
[16] V.I. Nefedov, I.S. Nefedova, Angular distribution of the photoelectrons from solids with account for elastic scattering and non-dipolar transitions, J. Electron Spectrosc. Relat. Phenom. 107 (2) (2000) 131–137.
[17] Jonas Weinen, Stefano Agrestini, Hidenori Fujiwara, Zhiwei Hu, Thomas C. Koethe, Yen-Fa Liao, Christian Schüßler-Langeheine, Ku-Ding Tsuei, Thomas Willers, Hua Wu, Liu Hao Tjeng, Hard X-ray photoelectron spectroscopy: New opportunities for chemical and physical analysis, Research Report Max-Plank-Institut für Chemische Physik Fester Stoffe, (2011), pp. 99–102.
[18] John P. Perdew, Kieron Burke, Matthias Ernzerhof, Generalized gradient approximation made simple, Phys. Rev. Lett. 77 (1996) 3865–3868.
[19] V.I. Anisimov, J. Zaanen, O.K. Andersen, Band theory and mott insulators: Hubbard U instead of stoner I, Phys. Rev. B 44 (1991) 943–954.
[20] C. Körber, V. Krishnakumar, A. Klein, G. Panaccione, P. Torelli, A. Walsh, J.L.F. Da Silva, S.-H. Wei, R.G. Egdell, D.J. Payne, Electronic structure of In_2O_3 and Sn-doped In_2O_3 by hard X-ray photoemission spectroscopy, Phys. Rev. B 81 (2010) 165207.